Achieving Sustainable Wood Preservation Using Nanomaterials

Nanomalzemeler Kullanılarak Sürdürülebilir Ahşap Koruma Sağlanması

Doğu RAMAZANOĞLU[1]

Abstract

In this study, a cost-effective and energy-efficient approach was used to impregnate the surface of solid wood with three different nanoparticle solutions and a hydrophobic polymer solution for wood protection. Impregnation of Ch, ZnO and SnO$_2$ nanoparticles increased the thermal stability of lignocellulosic materials, resulting in weight losses of 75.7-80.5% between 339-387°C. The binding of nanoparticles through impregnation also increased the water uptake rate, while silanization with HP increased hydrophobicity by 22.9-26.2%. The resulting wood was evaluated in terms of durability and performance as well as water and fire resistance, and it was predicted that it could be a sustainable approach to minimize the effects of adverse weather conditions on wood materials while reducing negative impacts on the environment and human health.

Keywords: Wood preservation, Nanomaterials, and Sustainable approaches

Özet

Bu çalışmada, masif ahşabın yüzeyini üç farklı nanopartikül çözeltisi ve ahşabın korunması için hidrofobik bir polimer çözeltisi ile emprenye etmek için uygun maliyetli ve enerji tasarruflu bir yaklaşım kullanılmıştır. Ch, ZnO ve SnO$_2$ nanopartiküllerinin emprenye edilmesi, lignoselülozik malzemelerin termal stabilitesini artırarak 339-387°C sıcaklıklar arasında %75,7-80,5 ağırlık kayıplarına neden olmuştur. Nanopartiküllerin emprenye yoluyla bağlanması da su alım oranını artırırken, HP ile silanizasyon hidrofobikliği %22,9-26,2 oranında artırmıştır. Elde edilen ahşap, su ve yangın direncinin yanı sıra dayanıklılık ve performans açısından değerlendirilmiş ve olumsuz hava koşullarının ahşap malzemeler üzerindeki etkilerini en aza indirirken çevre ve insan sağlığı üzerindeki olumsuz etkileri azaltmak için sürdürülebilir bir yaklaşım olabileceği öngörülmüştür.

Anahtar Kelimeler: Ahşap koruma, Nanomalzemeler ve Sürdürülebilir Yaklaşımlar

1. Introduction

Wood is a commonly used material for a range of applications such as furniture, construction, and paper production. However, its vulnerability to external factors like insects, water, and fire can have negative impacts on its aesthetic and structural properties. Traditional methods of protecting wood, such as chemical treatments and coatings, may have detrimental effects on both the environment and human health. Therefore, it is essential to explore more sustainable alternatives (Changotra et al., 2024; Raftery et al., 2024) to ensure the longevity and eco-friendliness of wood-based products.

One potential alternative is the use of nanotechnology in wood protection. By applying nanoparticles and nanocomposites to wooden surfaces (Ramazanoğlu, 2023a, 2023b) these materials can provide greater protection against decay and other types of damage while improving the mechanical properties of wood (Changotra et al., 2024; Raftery et al., 2024).

Biopolymers, such as chitin, chitosan, starch, gelatin, and zein, etc., represent a viable alternate solution for wood coating formulations both in terms of commercial and protective efficiency (Bulian & Graystone, 2009). One advantage of using biopolymers in wood conservation and protection is related to their high compatibility with polar adhesives. They also have improved biodegradability at the end of the life cycle, and the highly polar surface of the wood has a good affinity towards protein-based or cellulose derivate biopolymers.

Effective methods have been developed to address the challenges associated with using biopolymers in coatings formulations for wood protection. These challenges include insolubility in water, solubility in acid solutions, and high viscosity of their solutions. To overcome these challenges, ionic liquids have been employed as efficient solvent media for biopolymers. These techniques have been successfully applied to better preserve wood surfaces and protect against UV radiation (Croitoru et al., 2015; Garcia et al., 2010; Patachia et al., 2012).

Chitosan, a biopolymer derived from crustacean shells, has shown promise as a wood preservative either alone or as an additive in antifungal formulations (Alfredsen et al., 2004; Bhatt et al., 2024; Eikenes et al., 2005). Studies have found that chitosan with high molecular weight exhibits greater efficacy against wood decay fungi than chitosan with low molecular weight (Eikenes et al., 2005). Chitosan has also been studied as a potential protection agent against mold fungi such as Penicillium chrysogenum, Aspergillus flavus, and Aspergillus niger in historic artifacts located in dry Egyptian environments (El-Gamal et al., 2016). The concentration of chitosan was found to be positively correlated with its effectiveness in

protecting the wood against mold fungi for an efficient physical and chemical stabilization of chitosan on the wood surface that confers an enhanced antifungal protection, it is required to use it in combination with other polymers, e.g. polyethylene glycol (PEG), which initially reacts with wood, thus creating anchors for chitosan (Nowrouzi et al., 2016).

An interesting approach is to use lignin, a biopolymer isolated from the wood structure, as a UV stabilizer in wood coating formulations (Schaller & Rogez, 2007). Phenols leached from lignin can be absorbed by treated wood surfaces and act efficiently as biocides when testing against rot fungi (Chirkova et al., 2011). Lignin ester-based derivatives, such as lignin modified by reaction with lauroyl chloride, can be efficiently used as hydrophobization agents on the wood surfaces in protective coatings formulations (Gordobil et al., 2017). High performance coatings with improved thermal stability, better film-forming ability, enhanced hydrophobization action, as well as high adhesion towards wood surfaces are represented by high-lignin-content bio-based polyurethane systems (Griffini et al., 2015).

Ultrasonic waves can create a "sponge effect" in materials, similar to the motion of squeezing and releasing a sponge, which results in the rapid removal of moisture from a material immersed in liquid (Wan et al., 1992; Marangoni Júnior et al., 2023). This effect, in combination with the mechanical and physical effects of ultrasound, can contribute to many of the effects of diffusion (Floros & Liang, 1994). The resulting new microscopic channels in porous materials reduce the diffusion boundary layer and increase mass transfer (Tarleton, 1992; De la Fuente-Blanco et al., 2006; Ramazanoğlu et al., 2020b).

Recent studies have shown that using ultrasonic baths as a pretreatment can significantly reduce drying time and speed up the overall process(Ramazanoğlu et al., 2020a, 2020b) (Aversa et al., 2011; Jangam, 2011; Wang et al., 2024). This is due to several factors, including an increase in mass transfer rate (García-Pérez et al., 2009); (García-Pérez et al., 2011), enhanced water penetration (Bantle & Eikevik, 2011; He et al., 2017), an increase in wood-specific permeability coefficient (Han et al., 2023), loss of cellular adhesion, formation of wider cell gaps, rupture of cell walls, and formation of larger channels (He et al., 2017)

This study aims to increase the resistance of solid wood to water and fire by using the synergic effect of both positively charged biopolymer chitosan, ZnO, SnO_2 nanoparticles and synthetic hydrophobic polymer (HP) on the wooden surface without requiring additional energy under room conditions. The goal is to provide a more realistic, cost-effective, energy-efficient, and low-labor approach that can increase the competitiveness of large-scale production and provide affordable and high-quality materials for consumers.

The results indicate that the use of nanoparticles in the impregnation method partially increases the resistance of solid wood to water and fire under room conditions without requiring additional energy. This approach has the potential to provide a cost-effective and sustainable alternative for protecting wooden materials in large-scale applications. Furthermore, the use of nanotechnology can enhance the mechanical properties of wood and increase its durability, making it a more attractive option for the construction, furniture, and paper production industries.

2. Material and Method

2.1. Material

A local market was the source of 100% Birchwood wooden stirrers, which were produced from sapwood and were equally sized with a thickness of 1.00 mm, a width of 5.00 mm, and a length of 110 mm. These stirrers were used in this study. The required materials, including Chitosan (Cas no: 9012-76-4), Acetic acid (CH$_3$COOH % 99.8-100.5 Cas no: 27225-2.5L-R), and Hydrophobic polymer (HP), were also purchased from a local market. Additionally, TEKKIM company supplied TK.200650.05001 Ethyl alcohol (EtOH) 96% Teksoll Extra pure, TK.090250.05001 Isopropyl alcohol (2-Propanol), and TK.92008501002 Zinc Nitrate Hexahydrate [Zn(NO$_3$)$_2$.6H$_2$O] Extra pure, while MERCK company provided Tin(II) chloride dihydrate (SnCl$_2$.2H$_2$O). Color change measurements were conducted using a spectrophotometer device (PCE-CSM 10 model) at the FIBROBETON R&D center. Surface roughness measurements were taken using an optical profilometer device (Phase View brand), while thermogravimetric and differential thermal analyses (TGA/DTA) were performed using a device (DTG 60H - DSC 60TGA model / Shimadzu brand). Additionally, Scanning electron microscopy-energy dispersive X-ray analysis (SEM-EDX) imaging and measurements were carried out using equipment (FEI brand / Quanta FEG 250 model) at the Scientific and Technological Research Application and Research Center (DÜBİT).

2.2. Method

2.2.1. Preparation of wood samples

Using an ultrasonic frequency of 40 kHz, wood samples were subjected to a 15-minute washing cycle in an ultrasonic bath with pure water at a temperature of 25°C. Ramazanoğlu and Özdemir found that applying optimum ultrasonic conditions for 15 minutes at 25°C can result in an 80±2% reduction in drying time(Ramazanoğlu et al., 2020a). Ultrasonic baths are often used as a pretreatment in drying processes to reduce the overall processing time. This is because ultrasonic waves can create a "sponge effect" in materials, which can rapidly remove moisture and increase mass transfer, among other effects. Therefore, ultrasonic baths can be an effective and efficient method for reducing the drying time of materials.

A diagrammatic illustration outlining the procedure for creating the wooden substrate and solutions is presented in Figure 1.
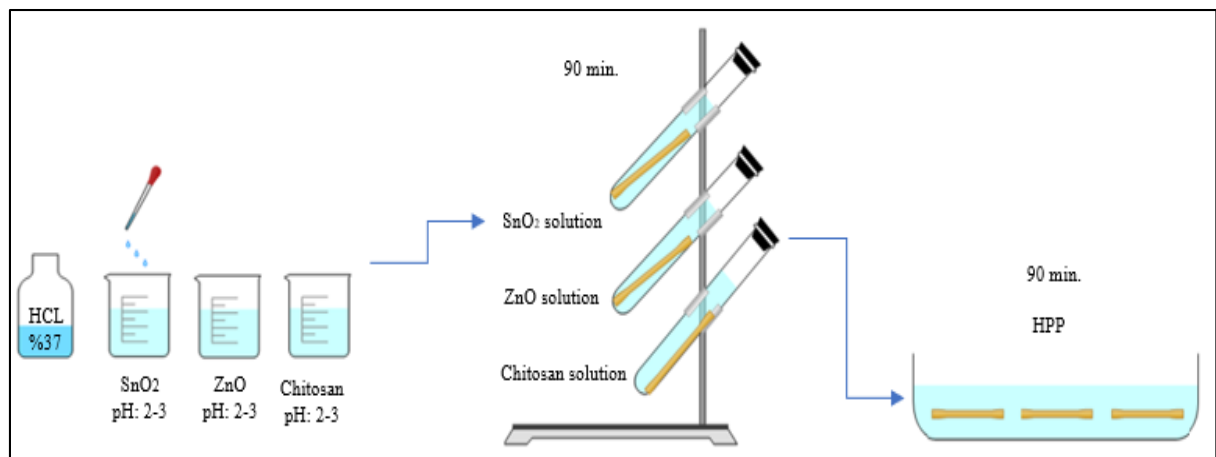

Figure 1. Displays a schematic representation of the process involved in producing the wooden substrate and solutions.

2.2.2. Preparation of solutions

Two solutions were prepared: a 200 mL solution of 0.5 M Zinc Nitrate [Zn $(NO_3)_2.6H_2O$] for application to wooden samples, and a 200 mL solution of 0.5 M Tin (II) Chloride Dihydrate ($SnCl_2.2H_2O$) in a water-to-ethanol ratio of 2:1. The process of preparing wooden surfaces and solutions is depicted in Figure 1.

The pH of the solutions was adjusted to 2-3 using 37% hydrochloric acid (HCl) to ensure the nanoparticles in the solution were positively charged (Figure 1). Next, wooden samples (1.00 X 5.00 X 110 mm) with negatively charged surfaces due to the presence of hydroxyl groups were submerged in three different solutions containing positively charged particles (Zhou & Fu 2020). The samples were left for 90 minutes, during which time the

positively charged particles were attracted to and adhered to the lignocellulosic surface of the wooden samples through electrostatic forces. Finally, the wood samples were rinsed with distilled water and dried in an oven at 60°C for 1 hour.

2.2.3. Color measurements

The color of wood is an important characteristic that can be affected by various factors, including surface functionalization. To measure color changes on lignocellulosic surfaces, the PCE-CSM 10 spectrophotometer was used in this study (Figure 2). It was applied to 7 samples, namely Wood (W), Wood-Chitosan (W-Ch), Wood-SnO$_2$ (W-SnO$_2$), Wood-ZnO(W-ZnO), Wood-Chitosan-HP (W-Ch-Si), Wood-SnO$_2$-HP (W-SnO$_2$-Si), and Wood-ZnO-HP (W-ZnO-Si. Each sample was repeated three times, and the average value was

calculated.

Figure 2. PCE-CSM 10 spectrophotometer.

This device measures color according to the CIE Lab* color space standard, which provides an
objective and standardized way of quantifying lightness (L*), red/green position (a*), and yellow/blue position (b*) for a given color. The L* value indicates the brightness value of a color, while the a* and b* values represent the color position on green-red and blue-yellow scales, respectively.

The CIE Lab* color space is widely used in industries such as printing, textiles, paint, and cosmetics to ensure accurate and consistent measurement and specification of color. This standard provides a reliable way of determining color differences and transmitting color information. Therefore, it has become a popular choice for color analysis in many fields Gilchrist and Nobbs, (1999).

2.2.4. Optical profilometer

The surface parameters obtained from the optical profilometry Phase View brand (Figure 3) include Sa, which represents the average apsidal height of the surface, Sq, which represents the average quadratic height, Ssk, which represents the slope of the surface, Sku, which represents the flatness, Sv, which represents the volumetric asymmetry, Sp, which represents the average volumetric asymmetry, St, which represents the total asymmetry value, and Sz, which represents the overall surface roughness average.

Figure 3. Optical Profilometer device.

As for the profile parameters: Ra represents the average surface roughness, Rq represents the root mean square deviation of the profile height from its mean line, Rsk represents the curvature of the profile, Rku (Kurtosis) represents a value that measures the conical accuracy of the surface texture relative to the mean line, Rv (Mean Depth of Surface Profile) represents the average roughness over the evaluation length, Rp (Peak-to-Valley Roughness) represents the maximum deviation of the profile height from its mean line over the evaluation length, representing the maximum surface roughness height, Rt (Total Roughness) represents the total height of the roughness, including peaks and valleys over the evaluation length, and Rz (Average Maximum Profile Height) represents the average of the Rti values calculated over the evaluation length, representing the average maximum value of the surface profile height.

2.2.5. TGA analysis

The TGA and DTA experiments were performed to study the thermal behavior of the samples. TGA was used to determine the amount and rate of weight loss, the temperatures at which degradation or decomposition occurs, and the residual weight after processing. DTA was used to identify phase changes and to determine the thermal properties of the samples.

For TGA analysis, a DTG-60H detector with a platinum cell was used in Düzce University. The experiments were conducted under a nitrogen atmosphere with a flow rate of 50 ml/min. The sample weight used for the analysis ranged between 6,000 to 9,000 mg.

Overall, the combination of TGA and DTA techniques provided valuable insights into the thermal stability and behavior of the samples.

2.2.6. SEM and EDX analysis

SEM and EDX analyses were conducted to examine the generated samples. The SEM images were obtained using the FEI Quanta FEG 250 model device located in the Central Research Laboratory at Duzce University. Prior to the SEM analysis, the samples were dried for 24 hours at 105°C. Since the samples had an insulating property, they were first made conductive and coated with a 5 nm thick layer of gold-palladium using a sputtering device in a suitable potential plasma environment before imaging. The coated samples were then placed on the microscope and stimulated with an area-emission gun at a specific height for imaging. Images were captured at both 30-micron and 300-micron sizes. EDX analysis was also performed to identify the elemental composition of the samples.

2.2.7. Water uptake (%)

The water uptake (%) values of the wood samples, which were measured by weighing after being soaked in water for 24 hours (Figure 19), were calculated using formula (1).

$$SW = \frac{Mw - Md}{Md} x\ 100$$

(1)

Where Md is the initial weight of the sample (g), Mw is the weight of the sample after immersion in water (g), and SW is the water uptake ratio (%).

3. Results and Discussion

3.1. SEM & EDX Analyses

The SEM and EDX images of the massive wood sample are presented in Figures 4-7. Figure 4 shows the elemental analyses of the wood surface with SEM and EDX images. The EDX spectrum in Figure 4 shows peaks for carbon (C) and oxygen (O), which are the main components of wood such as cellulose, hemicellulose, and lignin. The SEM image reveals that the lumens and channels are clearly visible without any coating or nano-accumulation on the wood surface.
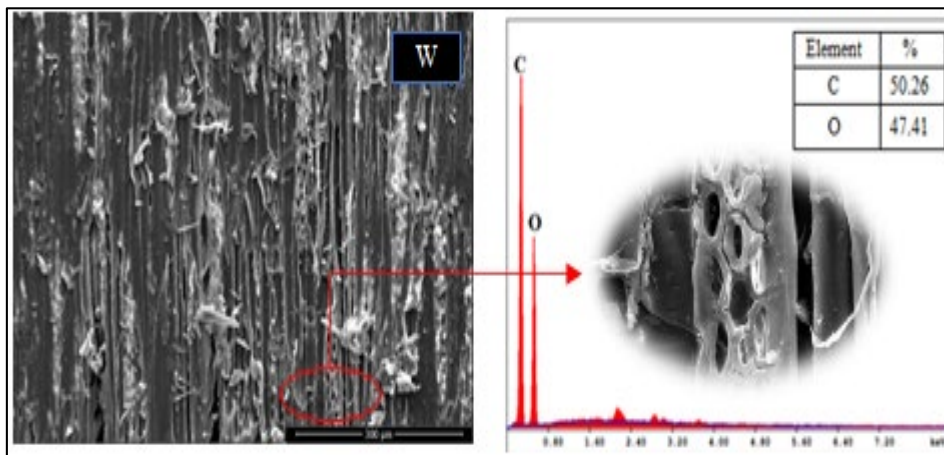

Figure 4. SEM and EDX images of the massive wood surface are presented with elemental analyses.

Figure 5 displays the SEM image and EDX analysis of the wood surface impregnated with chitosan solution positively charged by adding HCl for 90 minutes. The EDX spectrum analysis showed the emergence of the nitrogen (N) peak, indicating the attachment of chitosan to the lignocellulosic surface. The lumens were found to be closed due to the accumulation of chitosan on the surface.
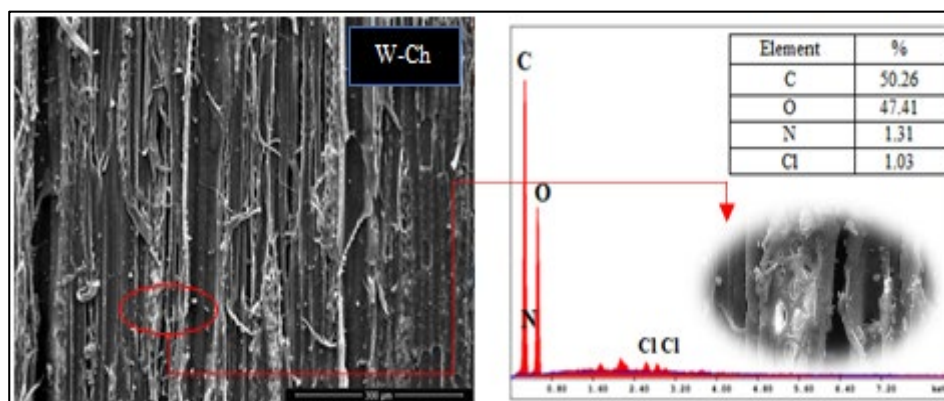

Figure 5. Elemental composition of the wood-chitosan (W-Ch) surface

In Figure 6, the SEM image and EDX analysis of the wood surface with positively charged ZnO nanoparticles accumulation are presented. The EDX spectrum analysis revealed that 42.35% C, 45.79 % O, and 9.76% Zn were adsorbed by the surface. The ZnO accumulations were observed to accumulate along the lumens and channels compared to the solid surface.
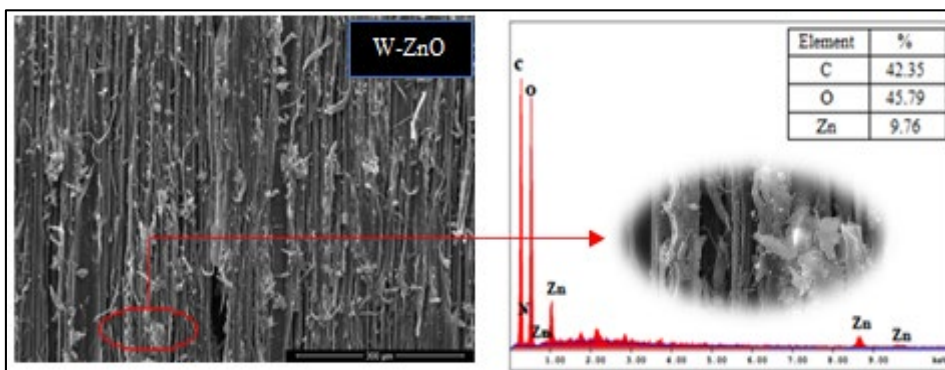

Figure 6. SEM and EDX analyses of the W-ZnO surface.

Figure 7 SEM and EDX analyses of the massive sample immersed in a solution containing positively charged SnO_2 particles. SEM and EDX analyses of the W-SnO_2 surface are depicted in indicating the presence of tiny particles on the wood surface.
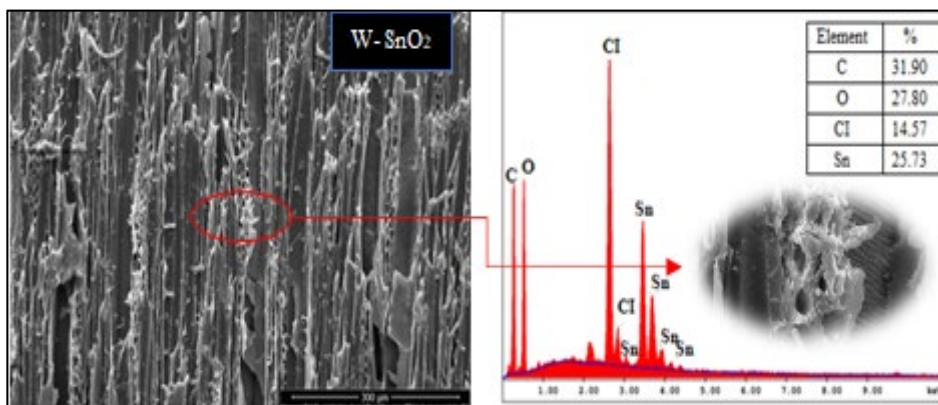
Figure 7. SEM and EDX analyses of the W-SnO_2 surface.

According to the EDX results, it was determined that tin (Sn) particles are located on the wood surface at a rate of 25.73% due to electrostatic forces of negatively charged hydroxyl groups. The SEM images also show SnO_2 particle adhesions.

Figures 8-10 display the SEM and EDX spectra obtained after the silanization of wood samples with HP.
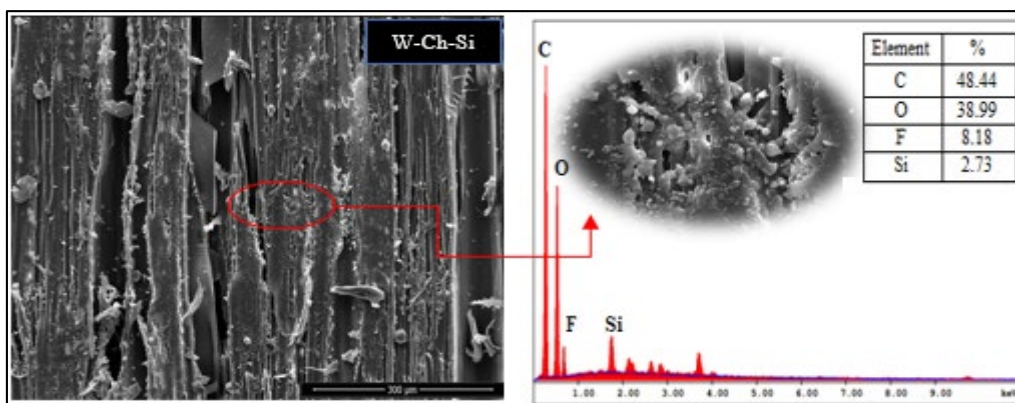
Figure 8. SEM and EDX analyses of the W-ZnO-Si surface.

The presence of F and Si peaks, which constitute 8.18% and 2.72%, respectively, indicates that HP adheres to the lignocellulosic surface where chitosan is located. The abundance of C and O peaks can be attributed to the presence of chitosan, while the typical cellulose peaks are also evident (Figure 8).
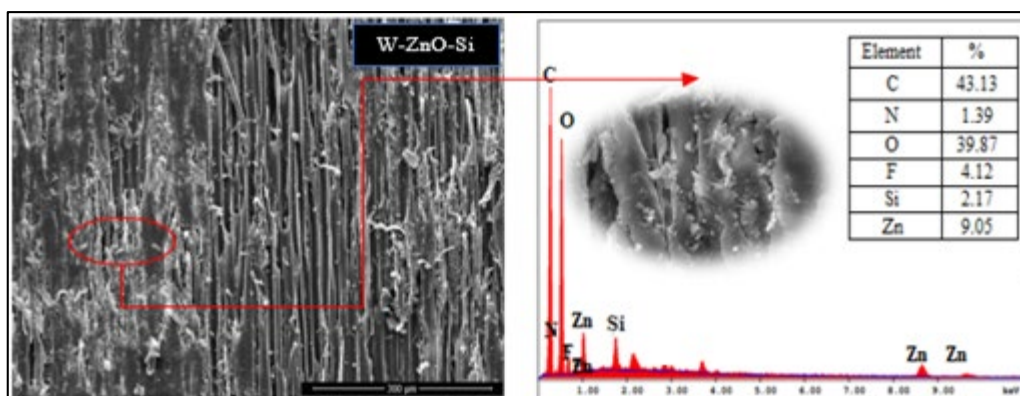

Figure 9. SEM and EDX analyses of the W-ZnO-Si surface.

Once again, it is feasible to detect Si and F peaks on the ZnO particle-functionalized wood surface, with values of approximately 2.17% and 4.12%, respectively. The occurrence of these peaks confirms that the surface has undergone hydrophobization, forming a top layer (Figure9).
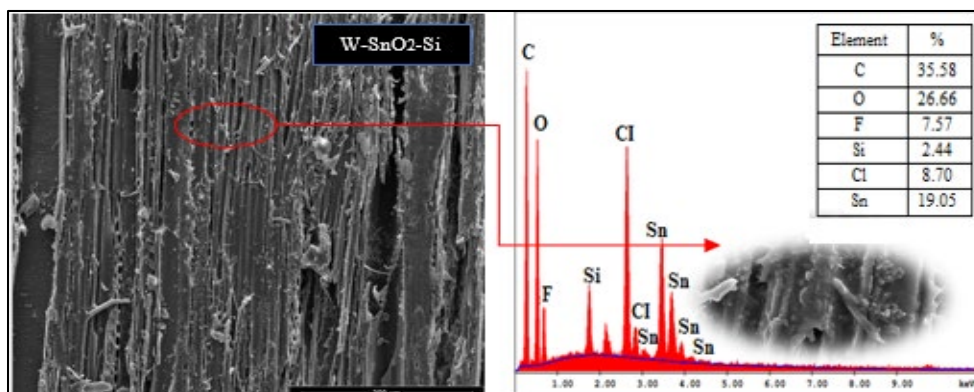

Figure 10. SEM and EDX analyses of the W-SnO$_2$-Si surface

Following silanization of the W-SnO$_2$ sample, peaks corresponding to F and Si were observed at 7.57% and 2.44%, respectively. Additionally, an 8.70% peak was detected, which is attributed to the presence of Tin(II) chloride salt. The peaks for C and O were identified as belonging to the lignocellulosic surface, representing 35.58% and 26.66%, respectively. SEM analysis revealed that the silanized surface exhibited a Waxy structure, characteristic of HP agents (Figure 10). This unique surface structure holds significant importance in creating biomimetic forms on various surfaces, as noted by (Ramazanoğlu and Özdemir, 2022).
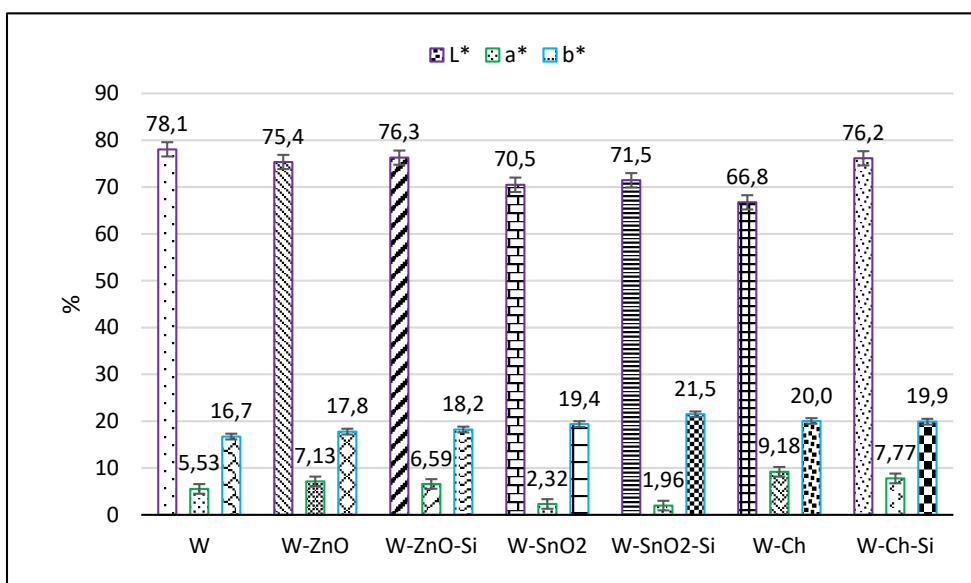

Figure 11. Color change parameters.

3.2. Color analysis

The color change parameters of the control sample were measured as L*, a*, and b* with values of 78.1%, 5.53%, and 16.7%, respectively. The wooden surface coated with ZnO particles exhibited a 3.87% decrease and measured 75.4% in the L* parameter, indicating whitening of the surface. The a* parameter, which represents changes in the red/green color tones, showed an increase of 28.9% and was measured as 7.13%. Meanwhile, the b* parameter, representing changes in yellow/blue tones, increased by 6.58% and was measured as 17.8%. Color parameter changes were observed in the wooden surface after each application.

The wooden surface functionalized with SnO$_2$ particles exhibited a decrease of 9.73% and 58.0% in L* and a* color parameters, respectively, which were found to be 70.5% and 2.32%, while the b* parameter showed an increase of 16.2% and was measured as 19.4%. The W-SnO$_2$-Si sample showed an 8.45% and 64.5% decrease and was observed as 71.5%

and 1.96% in L* and a* parameters, respectively. Meanwhile, the b* color parameter showed an increase of 28.7% and was calculated as 21.5%.

After the location of Ch particles, the L* value of the lignocellulosic surface was found to be 66.8%, which represented a 14.4% decrease. The a* and b* parameters increased by 66.0% and 19.7%, respectively, and were obtained as 9.18% and 20.0%. The W-Ch-Si sample exhibited a 2.43% decrease in L* value, and an increase of 40.5% and 19.1% in a* and b* parameters, respectively. These values were also recorded as 7.77% and 19.9%, respectively (Figure 11). As seen, these color parameter changes are specifically attributed to the nanoparticles, which can be evaluated as characteristic properties (Ramazanoğlu et al., 2020b).

3.3. Optical Profilometer

Optical profilometry is a non-contact measurement technique used to determine the surface profile, height, and shape of objects. The profilometer shines light onto the surface of the object and measures the amount of reflected light. This information is then used to create a three-dimensional image of the surface, which can be used for various purposes such as determining surface roughness, detecting surface defects, and measuring surface heights.In this study, evaluating the surface morphology through the surface roughness parameters of Ra and Rz would be a more objective approach.
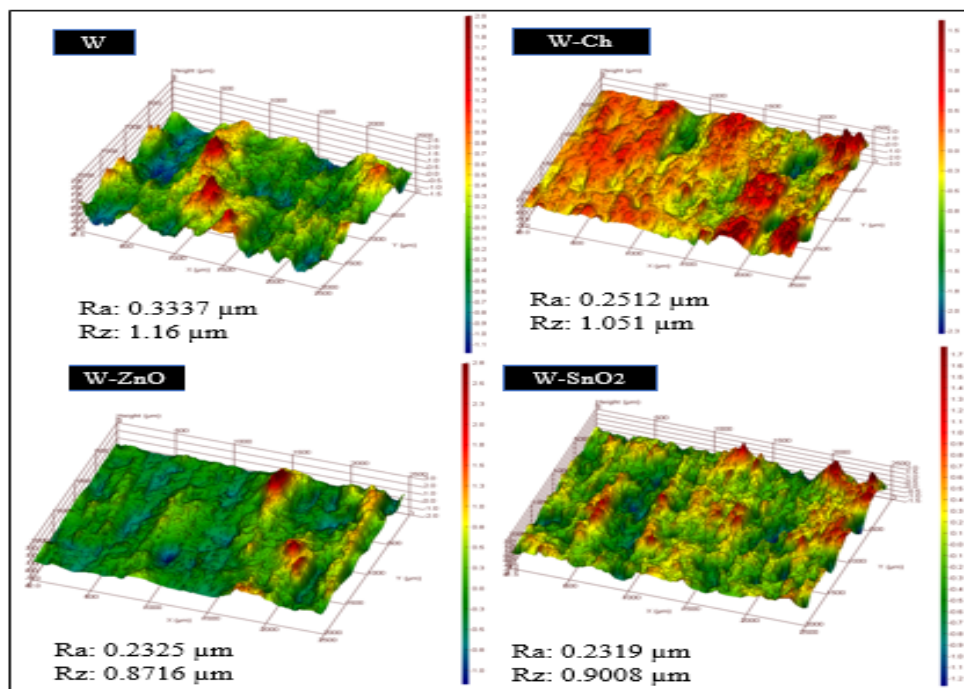

Figure 12. Illustrates the surface roughness of the massive(W), chitosan-treated (W-Ch), Zinc Oxide-treated (W-ZnO), and Tin Oxide-treated (W-SnO$_2$) samples, respectively.

The surface profile parameters of the untreated bulk control sample were measured as Ra: 0.3337 µm and Rz: 1.16 µm (Figure 12). The surface parameter values for the W-Ch sample treated with positively charged chitosan particles were determined as Ra: 0.2512 µm and Rz: 1.051 µm (Figure 10). It was observed that after impregnation of the surface with chitosan, there was a 24.7% decrease in the arithmetic average roughness value Ra, while the average maximum height of the profile decreased by 30.3% compared to the bulk due to the location of Zinc Oxide (ZnO) particles on the wood surface, with Ra decreasing to 0.2325 µm and Rz decreasing by 24.8% to 0.8716 µm. Following impregnation with a tin solution, the surface parameter values were found to be Ra: 0.2319 µm and Rz: 0.9008 µm, respectively, indicating a decrease of 30.5% and 22.3% (Figure 12).

After silanization, the surface roughness of samples treated with Zinc Oxide (W-ZnO), Tin Oxide (W-SnO$_2$), and Chitosan (W-Ch), respectively, was measured and recorded in Figure 13.
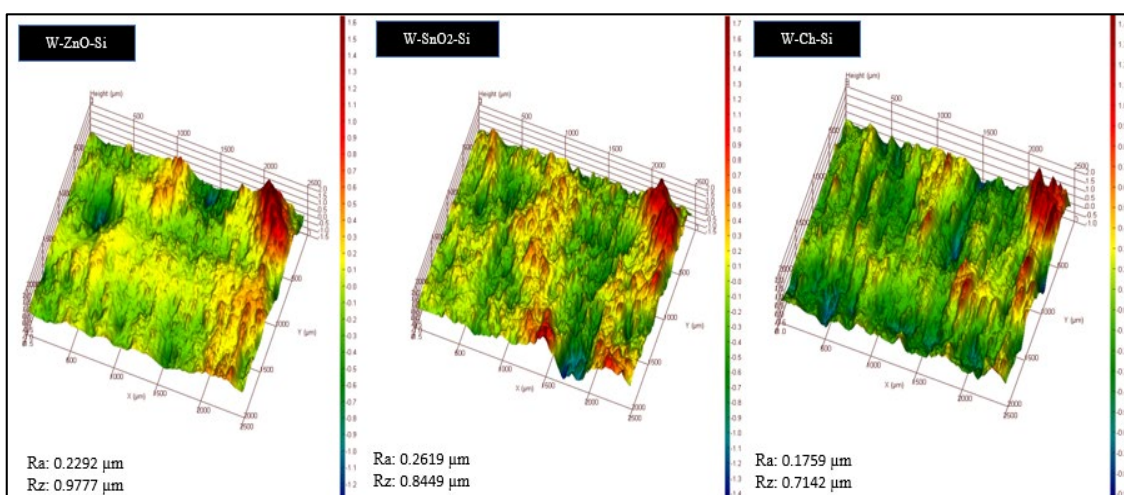

Figure 13. Surface roughness values of samples after silanization.

The surface tension of whole samples is illustrated in Figure 14.

Figure 14. The surface tension of whole samples.

Following the hydrophobization of the ZnO-treated surface using HP, a decrease of 1.41% was observed in the average surface roughness parameter Ra, resulting in a value of 0.2292 µm. In contrast, the Rz value increased by 12.2% to 0.9777 µm. The roughness parameters Ra and Rz for W-SnO$_2$-Si were determined as 0.2619 µm and 0.8449 µm, respectively, and are depicted in Figure 11. The roughness parameters for W-Ch-Si samples were calculated as Ra: 0.1759 µm and Rz: 0.7142 µm, indicating a reduction of approximately 29.9% and 32.0%, respectively, due to the formation of the HP's waxy top layer (Ramazanoğlu & Özdemir, 2022a). This biomimetic surface topography is essential for surface tension, as illustrated in Figure 14.

3.4. Thermogravimetric analysis

Thermogravimetric analysis (TGA) is a widely used analytical technique that measures how the weight of a sample changes with temperature. It is employed to study the thermal behavior of materials, including the amount and rate of weight loss, the temperatures at which degradation or decomposition occurs, and the residual weight after processing. TGA finds broad applications in various fields, such as materials science, chemistry, and environmental science, to determine thermal stability, composition, and assess the purity and contamination of materials. The technique is based on the principle that the weight of a sample changes due to physical or chemical processes (such as evaporation, oxidation, and decomposition) resulting from heating. In this study, the thermal stabilization of wood samples functionalized with nanoparticles in surface impregnation was compared. Figure 15 presents the TGA and DTA graphs for solid wood after Tin and HP treatment. After acumulation of Ch, ZnO and SnO$_2$ nanoparticles on lignoselülosic surfaces TGA and DTA spectrums were given Figures 15-16.
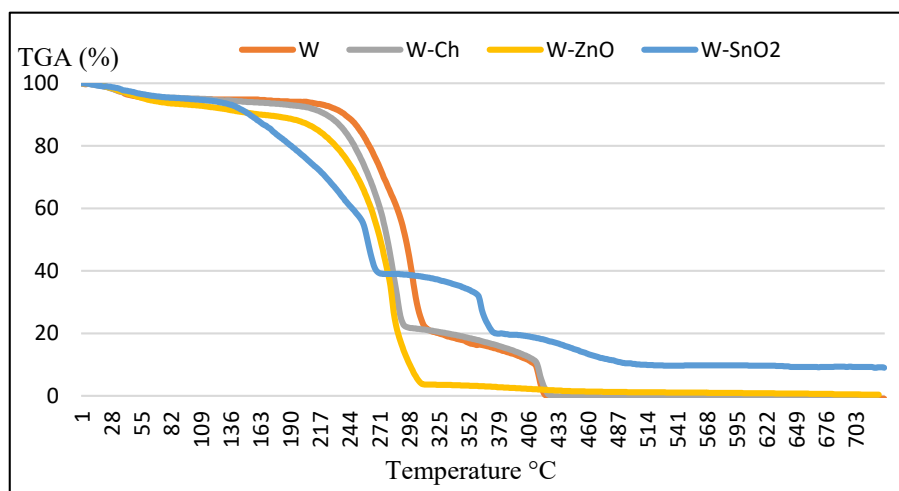

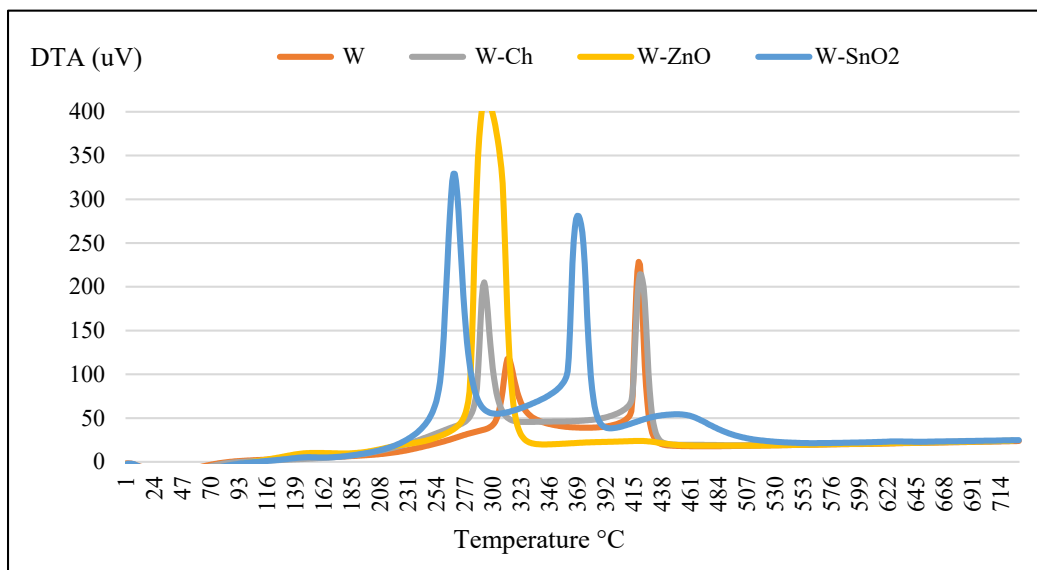**Figure 15.** TGA spectra of the treated surface with nanoparticles.

Figure 16. DTA spectra of the treated surface with nanoparticles.

The TGA curves of the Control (W) and functionalized W-Ch, W-ZnO, and W-SnO2 samples exhibit similar weight loss up to 100°C (Figure 13). This may be attributed to the departure of water molecules from the lignocellulosic structure (Ramazanoğlu & Özdemir, 2022b). The shoulder observed at 350-363°C in the massive sample (W) could be due to the depolymerization of hemicellulose, resulting in a weight loss of 37.6%, while the second largest decomposition peak at 458-478°C may be attributed to cellulose degradation, causing a weight loss of 16.7%. The hemicellulose loss in the W-ZnO sample occurred at temperatures ranging from 338-387°C with a weight loss of 85.4%, while a possible cellulose decomposition was indicated by a weight loss of approximately 2.07% between 365-462°C (Figure 16). Figure 17 displays the TGA spectra of the wood samples that underwent hydrophobization, while Figure 16 shows the DTA spectra of the samples after silanization.
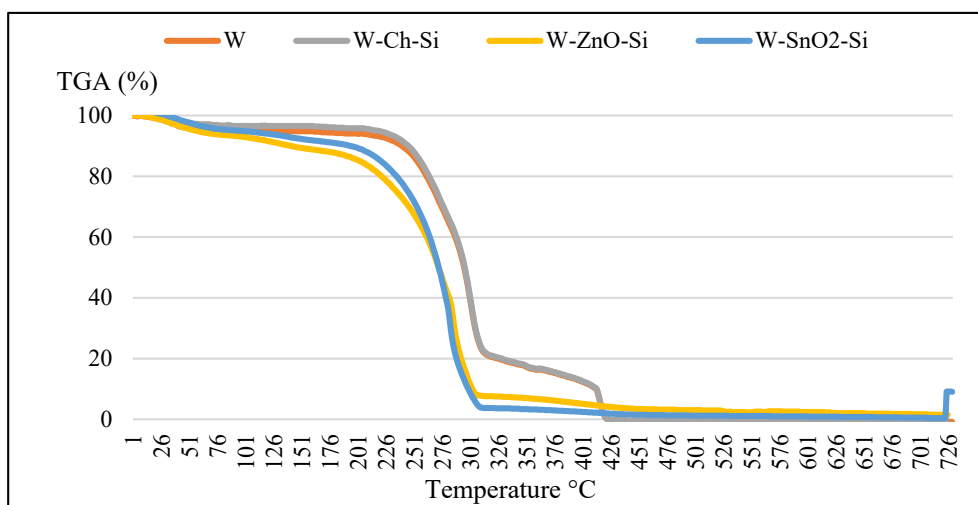

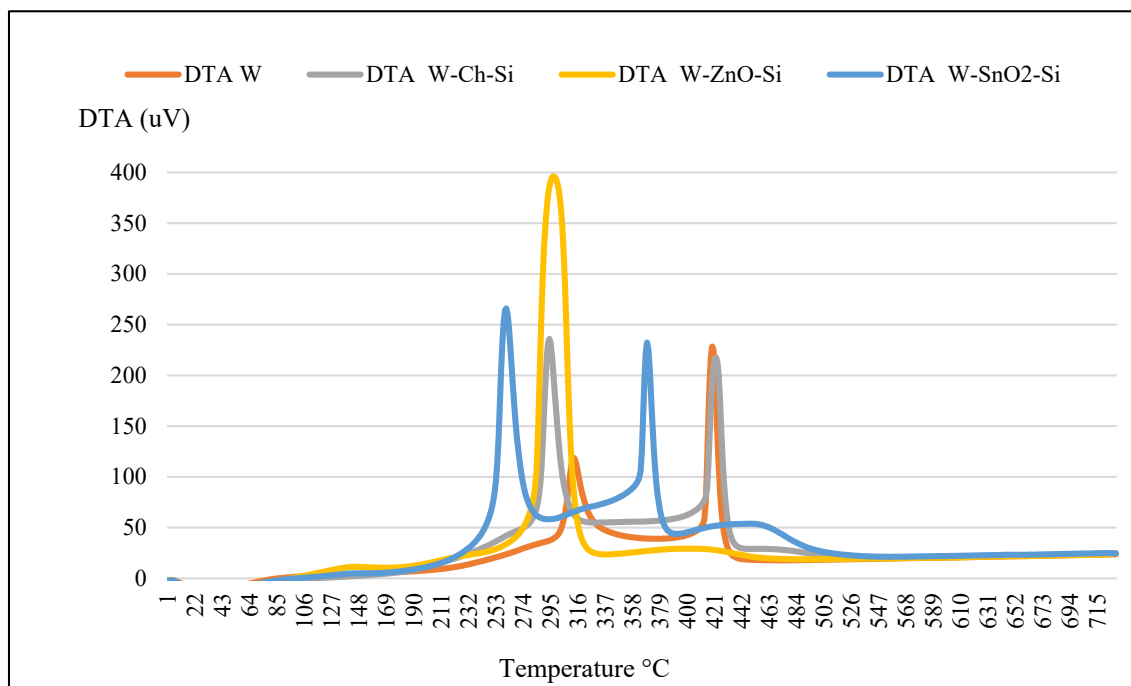**Figure 17.** TGA spectra of the wood samples after hydrophobization.

Figure 18. DTA spectra of the samples following silanization.

After silanization with HP, the W-Ch-Si sample exhibited a weight loss of 75.7% between temperatures of 339-363°C, and a weight loss of 16.5% at 482°C, which was likely attributed to functional groups outside of the biomass. In the case of W-SnO$_2$-Si, the first weight loss of 34.8% was observed between 306-333°C, followed by a second weight loss of 18.9% between 417-435°C. For the W-ZnO-Si sample, a weight loss of 80.5% was observed between 338-387°C, while a weight loss of 4.24% occurred between 372-445°C (figures 17-18).

For the W-Ch-Si sample:

➢ A weight loss of 75.7% between temperatures of 339-363°C
➢ A weight loss of 16.5% at 482°C

For the W-SnO$_2$-Si sample:

➢ The first weight loss of 34.8% was observed between 306-333°C
➢ A second weight loss of 18.9% between 417-435°C

For the W-ZnO-Si sample:

➢ A weight loss of 80.5% was observed between 338-387°C
➢ A weight loss of 4.24% occurred between 372-445°C

Based on the weight loss patterns provided, the samples can be ranked in order of thermal stability. The most stable sample is W-SnO$_2$-Si because it exhibits weight loss at the highest

temperature. The second most stable sample is W-Ch-Si, and the least stable sample is W-ZnO-Si because it exhibits weight loss at the lowest temperature. This ranking provides valuable information for selecting the most suitable wood protection approach for specific applications. It also highlights the potential of nanoparticle impregnation with hydrophobic polymer for enhancing the thermal stability of lignocellulosic materials, which is a key factor in preventing the negative effects of adverse weather conditions.

3.5. Water uptake (%)

The bar chart above illustrates the water absorption values of test and control samples under different conditions. The first bar represents the massive sample (W) immersed in water for 24 hours, which showed a 61% increase in water absorption. The next three bars represent samples functionalized with chitosan (Ch), zinc oxide (ZnO), and tin dioxide (SnO_2) nanoparticles. These samples exhibited increased hydrophilicity, as indicated by the respective increases in water absorption values of 71.0%, 73.0%, and 64.0%. The last three bars represent the samples that underwent silanization with HP, which resulted in lower water absorption values of 47.0%, 46.0%, and 45.0% (Ramazanoğlu & Özdemir 2021; Ramazanoğlu et al., 2022) After silanization, the hydrophobicity of samples W-Ch-Si, W-ZnO-Si, and W-SnO_2-Si was improved by 22.9%, 24.5%, and 26.2% respectively.
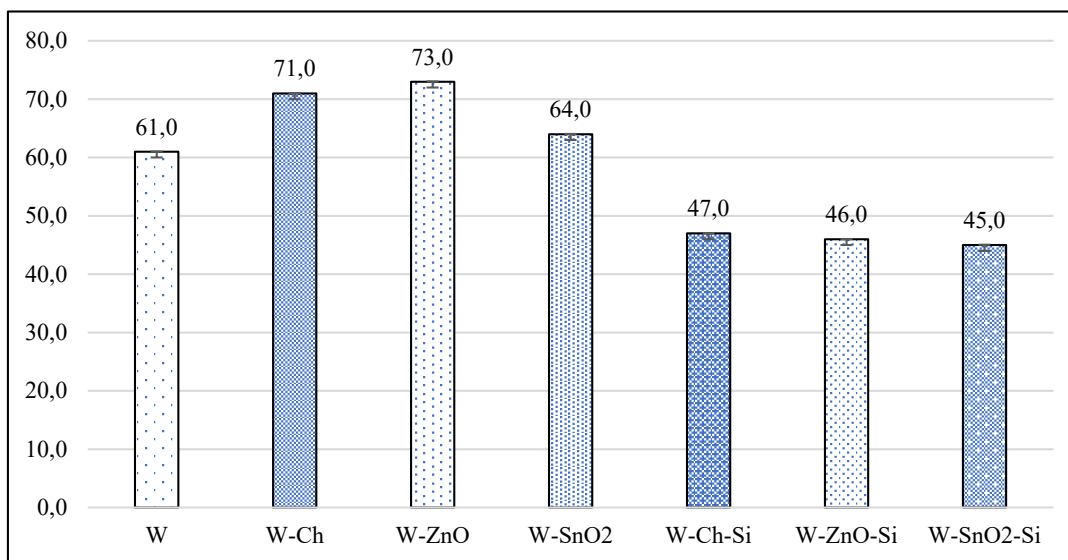

Figure 19. Water intake rations (%)

The study suggests that functionalizing massif samples with nanoparticles can increase their hydrophilicity, while silanization with HP can reduce it. These findings have important implications for developing materials with controlled hydrophilicity with various applications.

4. Results

According to TGA and DTA analysis, the mass loss of untreated wood (W) started earlier than the functionalized samples. The shoulder observed at 350-363°C in the massive sample (W) could be due to the depolymerization of hemicellulose, resulting in a weight loss of 37.6%, while the second largest decomposition peak at 458-478°C may be attributed to cellulose degradation, causing a weight loss of 16.7%. The weight loss for the W-Ch-Si sample was 75.7% between temperatures of 339-363°C, and a weight loss of 16.5% at 482°C. For the W-ZnO-Si sample, a weight loss of 80.5% was observed between 338-387°C, while a weight loss of 4.24% occurred between 372-445°C. The weight loss for the W-SnO$_2$-Si sample was 34.8% between 306-333°C, followed by a weight loss of 18.9% between 417-435°C. After silanization, the hydrophobicity of samples W-Ch-Si, W-ZnO-Si, and W-SnO$_2$-Si was improved by 22.9%, 24.5%, and 26.2% respectively. In terms of fire resistance, the most stable sample was W-SnO$_2$-Si, with a weight loss of 18.9% between 417-435°C, followed by W-Ch-Si with a weight loss of 16.5% at 482°C, and the least stable was W-ZnO-Si, with a weight loss of 4.24% between 372-445°C. Overall, the attachment of nanoparticles to the surface through the impregnation method was successful, resulting in improved thermal stability and water resistance. The addition of hydrophobic agents such as HP has further enhanced the resistance against combustion, making this wood protection method with nanoparticles highly cost-effective in terms of energy and labor.

Acknowledgments

References

Alfredsen, G., Eikenes, M., Militz, H., & Solheim, H. (2004). Screening of chitosan against wood-deteriorating fungi. *Scandinavian Journal of Forest Research*, *19*, 4–13.

Aversa, M., van der Voort, A. J., de Heij, W., Tournois, B., & Curcio, S. (2011). An Experimental Analysis of Acoustic Drying of Carrots: Evaluation of Heat Transfer Coefficients in Different Drying Conditions. *Drying Technology*, *29*(2), 239–244.

Bantle, M., & Eikevik, T. M. (2011). Parametric Study of High-Intensity Ultrasound in the Atmospheric Freeze Drying of Peas. *Drying Technology*, *29*(10), 1230–1239.

Bhatt, S., Pathak, R., Punetha, V. D., & Punetha, M. (2024). Chitosan nanocomposites as a nano-bio tool in phytopathogen control. *Carbohydrate Polymers*, *331*, 121858.

Bulian, F., & Graystone, J. A. (2009). Wood coatings: Theory and practice. *Wood Coatings: Theory and Practice*, 1–320.

Changotra, R., Rajput, H., Liu, B., Murray, G., & He, Q. (Sophia). (2024). Occurrence, fate, and potential impacts of wood preservatives in the environment: Challenges and environmentally friendly solutions. *Chemosphere*, *352*, 141291.

Chirkova, J., Andersone, I., Irbe, I., Spince, B., & Andersons, B. (2011). Lignins as agents for bio-protection of wood. *Holzforschung*, *65*(4), 497–502.

Croitoru, C., Patachia, S., & Lunguleasa, A. (2015). A mild method of wood impregnation with biopolymers and resins using 1-ethyl-3-methylimidazolium chloride as carrier. *Chemical Engineering Research and Design*, *93*, 257–268.

De la Fuente-Blanco, S., Riera-Franco de Sarabia, E., Acosta-Aparicio, V. M., Blanco-Blanco, A., & Gallego-Juárez, J. A. (2006). Food drying process by power ultrasound. *Ultrasonics*, *44*(SUPPL.), e523–e527.

Eikenes, M., Alfredsen, G., Christensen, B. E., Militz, H., & Solheim, H. (2005). Comparison of chitosans with different molecular weights as possible wood preservatives. *Journal of Wood Science*, *51*(4), 387–394.

El-Gamal, R., Nikolaivits, E., Zervakis, G. I., Abdel-Maksoud, G., Topakas, E., & Christakopoulos, P. (2016). The use of chitosan in protecting wooden artifacts from damage by mold fungi. *Electronic Journal of Biotechnology*, *24*, 70–78.

Floros, J. D., & Liang, H. (1994). *Acoustically assisted diffusion through membranes and biomaterials*. https://research.polyu.edu.hk/en/publications/acoustically-assisted-diffusion-through-membranes-and-biomaterial.

Garcia, H., Ferreira, R., Petkovic, M., Ferguson, J. L., Leitão, M. C., Gunaratne, H. Q. N., Seddon, K. R., Rebelo, L. P. N., & Silva Pereira, C. (2010). Dissolution of cork biopolymers in biocompatible ionic liquids. *Green Chemistry*, *12*(3), 367–336.

García-Pérez, J. V., Cárcel, J. A., Riera, E., & Mulet, A. (2009). Influence of the Applied Acoustic Energy on the Drying of Carrots and Lemon Peel. *Drying Technology*, *27*(2), 281–287.

García-Pérez, J. V., Ozuna, C., Ortuño, C., Cárcel, J. A., & Mulet, A. (2011). Modeling Ultrasonically Assisted Convective Drying of Eggplant. *Drying Technology*, *29*(13), 1499–1509.

Gordobil, O., Herrera, R., Llano-Ponte, R., & Labidi, J. (2017). Esterified organosolv lignin as hydrophobic agent for use on wood products. *Progress in Organic Coatings*, *103*, 143–151.

Griffini, G., Passoni, V., Suriano, R., Levi, M., & Turri, S. (2015). Polyurethane coatings based on chemically unmodified fractionated lignin. *ACS Sustainable Chemistry & Engineering*, *3*(6), 1145–1154.

Han, T., Lu, M., Cui, S., Liu, S., Avramidis, S., & Qian, J. (2023). How does ultrasound contribute to the migration of extractives inside Ailanthus altissima wood? *Ultrasonics Sonochemistry*, *101*, 106708.

He, Z., Wang, Z., Zhao, Z., Yi, S., Mu, J., & Wang, X. (2017). Influence of ultrasound pretreatment on wood physiochemical structure. *Ultrasonics Sonochemistry*, *34*, 136–141.

Jangam, S. V. (2011). An Overview of Recent Developments and Some R&D Challenges Related to Drying of Foods. *Drying Technology*, *29*(12), 1343–1357.

Marangoni Júnior, L., Augusto, P. E. D., Vieira, R. P., Borges, D. F., Ito, D., Teixeira, F. G., Dantas, F. B. H., & Padula, M. (2023). Food-Package-Processing relationships in emerging technologies: Ultrasound effects on polyamide multilayer packaging in contact with different food simulants. *Food Research International*, *163*, 112217.

Nowrouzi, Z., Mohebby, B., & Younesi, H. (2016). Treatment of fir wood with chitosan and polyethylene glycol. *Journal of Forestry Research*, *27*(4), 959–966.

Patachia, S., Croitoru, C., & Friedrich, C. (2012). Effect of UV exposure on the surface chemistry of wood veneers treated with ionic liquids. *Applied Surface Science*, *258*(18), 6723–6729.

Raftery, G. M., Karami, Z., & Nicholson, C. L. (2024). Natural ageing of one-component polyurethane bonded preservative treated wood evaluated using fracture energy tests. *International Journal of Adhesion and Adhesives*, *132*, 103681.

Ramazanoğlu, D. (2023a). Composite Materials in Biomimetic Nanohybrid Structures for Analytical Chemistry, Surface Chemistry, and Corrosion. In *Farklı Mühendislik Yaklaşımlarıyla Kompozit Malzemeler- I*. Özgür Yayınları.

Ramazanoğlu, D. (2023b). Nanotechnology and Architecture: Applications and Potential of Nanocomposites. In *Farklı Mühendislik Yaklaşımlarıyla Kompozit Malzemeler-II*. Özgür Yayınları.

Ramazanoğlu, D., & Özdemir, F. (2021). ZnO-based Nano Biomimetic Smart Artificial Form Located on Lignocellulosic Surface with Hydrothermal Approach. *Kastamonu University Journal of Forestry Faculty*, *21*(1), 12–20.

Ramazanoğlu, D., & Özdemir, F. (2022a). Biomimetic surface accumulation on Fagus orientalis. *Applied Nanoscience (Switzerland)*, *12*(8), 2421–2428.

Ramazanoğlu, D., Mohammed, Z. A., Khalo, I., & Maher, K. (2022). Aubergine-based Biosorbents for Heavy Metal Extraction. *Bayburt Üniversitesi Fen Bilimleri Dergisi*, *5*(2), 198–205.

Ramazanoğlu, D., Özdemir, F., (2020a). Ahşap Yüzeyde Akıllı Nano Biyomimetik Hidrotermal Lokasyonlama. *Bartın Orman Fakültesi Dergisi*, *22*(2), 447–456.

Ramazanoğlu, D., Özdemir, F., (2020b). Ön İşlem Olarak Uygulanan Ultrasonik Banyonun Ceviz Kaplamaların Özellikleri Üzerine Etkileri. *Bartın Orman Fakültesi Dergisi*, *22*(2), 479–484

Schaller, C., & Rogez, D. (2007). New approaches in wood coating stabilization. *Journal of Coatings Technology and Research*, *4*(4), 401–409.

Tarleton, E. S. (1992). The role of Field-assisted techniques in solid/liquid separation. *Filtration & Separation*, *29*(3), 246–238.

Wan, P. J., Muanda, M. wa, & Covey, J. E. (1992). Ultrasonic vs. nonultrasonic hydrogenation in a batch reactor. *Journal of the American Oil Chemists Society*, *69*(9), 876–879.

Wang, K., He, P., Wang, Q., Yang, Z., Xing, Y., Ren, W., Wang, J., & Xu, H. (2024). Ultrasound pretreatment enhances moisture migration and drying quality of mulberry via microstructure and cell-wall polysaccharides nanostructure modification. *Food Research International*, *184*, 114245.

Zhou, L., & Fu, Y. (2020). Flame-retardant wood composites based on immobilizing with chitosan/sodium phytate/nano-TiO_2-ZnO coatings via layer-by-layer self-assembly. *Coatings, 10*(3), 296. MDPI AG.